

The impact of cooling rate and hydrogen concentration on hydride morphology in Zircaloy-4

Peter Kaufholz
BGZ Gesellschaft für
Zwischenlagerung mbH

Maik Stuke
BGZ Gesellschaft für
Zwischenlagerung mbH

Timo Neikes
BGZ Gesellschaft für
Zwischenlagerung mbH

Felix Boldt
BGZ Gesellschaft für
Zwischenlagerung mbH

Anna-Maria Alvarez
Studsvik Nuclear AB

Mathias Segerberg
Studsvik Nuclear AB

Abstract

Hydride re-orientation may reduce ductility in zirconium-based cladding materials during extended dry storage. Therefore, investigations on hydrogen behavior are crucial to ensure safety of dry storage over extended time spans. This study investigates hydrogen behavior in un-irradiated Zircaloy-4 cladding tubes under conditions relevant to interim dry storage focusing on hydrogen precipitation, diffusion and hydride morphology. The effects of cooling rate and total hydrogen concentration on zirconium hydride morphology were investigated by exposing samples of certain hydrogen concentrations to varying cooling rates. Experiments were conducted, giving particular interest to hydride morphology under four distinct cooling rates across four hydrogen concentrations. In addition, a hydrogen diffusion experiment on an un-irradiated pre-hydrided tube segment exposed to a constant temperature gradient was performed to investigate on axial hydrogen redistribution.

Results indicate a significant influence of cooling rate on zirconium hydride precipitation. The number of hydrides was found to increase with increasing cooling rate, while the size of hydrides decreases. Furthermore, an orientation effect was observed, showing randomly oriented hydrides for fast cooling, while slow cooling leads to long circumferential oriented hydrides. An increase in hydrogen concentration leads to a higher number of hydrides, with a notable reduction in the impact of concentration at faster cooling rates. Samples with hydrogen concentrations above hydrogen solubility were assumed to contain non-dissolved hydrides at the maximum test temperature. For those samples the impact of cooling rate on hydrogen size and number was minimized, showing no variation in hydride size and number throughout different cooling rates. The experiment on hydrogen diffusion along a constant temperature gradient showed a reversal in the hydrogen concentration gradient of the specimen. Also, the final hydrogen gradient as a result of thermo diffusion was found to be small and within the measurement uncertainties of the method.

These results underscore the importance of realistic boundary conditions for dry storage safety assessments. The findings also provide valuable input for experiments

involving spent nuclear fuel such as BGZ's research project LEDA (Long-term Experimental Dry storage Analysis).

1 - Introduction

Understanding the behaviour of hydrogen in nuclear fuel rods is essential for ensuring the safety of dry stored nuclear fuel assemblies [1, 2]. This research focuses on the diffusion and precipitation of hydrogen in unirradiated Zircaloy-4 cladding tubes, with particular emphasis on conditions relevant to interim dry storage scenarios [3, 4]. By obtaining experimental data on hydrogen behaviour, we aim to extend the validation base for existing models that predict hydrogen diffusion and precipitation, which are critical for the structural integrity and performance of fuel rods during dry storage [5]. The results of the work at hand contribute to the determination of test conditions for future investigations on used fuel rods from nuclear power reactors.

In addition to the hoop stress and total hydrogen concentration, the cooling rate affects the morphology of zirconium hydrides, the precipitated forms of hydrogen within the cladding material [6–14]. However, cooling rates during dry storage are in the range of several °C/year being far too slow for direct examinations using irradiated fuel rods within hot cell laboratories. Nevertheless, an alternative approach can be followed by observing the effect of different slow cooling rates on hydride morphology.

Due to the anisotropy of α -zirconium matrix and its preferred orientation in zirconium based cladding tubes, the preferentially formed δ -zirconium hydrides precipitate in circumferential orientation [12, 15].

The primary objective of this study is to investigate how different cooling rates and hydrogen concentrations affect the size and morphology of zirconium hydrides. We investigated 16 cladding samples with defined combinations of four different hydrogen concentrations and cooling rates.

Additionally, this research will examine the hydrogen concentration profile along the axial direction of an unirradiated cladding tube exposed to a heat treatment under a constant temperature profile.

The experimental setup and methodologies of this study serve a dual purpose: Besides addressing the immediate goals concerning unirradiated Zircaloy-4 cladding tubes, they also act as a preliminary study for future investigations involving irradiated fuel rods. This research is crucial as it will provide deeper insights into the behaviour of hydrogen in cladding materials subjected to the more complex and demanding conditions present after irradiation.

2 - Material and Methods

The experiments were performed on un-irradiated cold worked stress relief (CWSR) annealed Zircaloy-4 cladding tubes according to the ASTM standard [16]. We prepared 40 mm long cladding tube samples to investigate the impact of different cooling rates and hydride concentrations on the hydride morphology. One further sample of 190 mm length has been prepared to investigate axial hydrogen diffusion.

The hydrogen concentration has been determined by hot extraction (HE) in an inert gas using an Elementrac OH-p2 [17]. For the microscopic investigations etching was

performed using a combination of H₂SO₄, H₂O₂ and H₂O. The micrographs have been taken using a Leica MeF-4 inverted microscope [18].

Morphology experiment				
c _H [wt. ppm]	Cooling rates [°C/h]			
38 ±5	150	12.5	1.8	0.4
52 ±5	150	12.5	1.8	0.4
96 ±5	150	12.5	1.8	0.4
267 ±5	150	12.5	1.8	0.4

Diffusion experiment				
Length [mm]	c _H ^{left} [wt. ppm]	c _H ^{right} [wt. ppm]	T _{max} [°C]	T _{grad} [°C/cm]
190	59 ±5	98 ±5	349	2.59

Table 1: Test matrix containing morphology experiments and the diffusion experiment on Zircaloy-4 cladding. The morphology experiments include 40 mm long samples with four different hydrogen concentrations being subject to four different cooling rates, each. The diffusion experiment was performed on a 190 mm long sample with an initial hydrogen concentration gradient from left to right exposed to a temperature gradient.

2.1 Hydride Morphology Experiments

Four samples were charged with hydrogen using atmospheric charging in an Ar/H₂ mixture. The charged samples were homogenized at 450 °C for two weeks. The cooling rate following the homogenization treatment was 480 °C per hour. It is assumed that the homogenization procedure does not change the microstructure of the sample significantly due to an even higher temperature during the cladding material production process including a final heat treatment of 480 °C for several hours. Final hydrogen levels of the 4 samples were determined to be 38, 52, 96 and 267 weight-ppm hydrogen (±5 ppm) respectively. At the maximum test temperature of 347 °C we assume all hydrogen to be dissolved for the three lower concentrations. The sample containing 267 ppm of hydrogen is considered to contain residual hydrides at the maximum test temperature. Thus, a different precipitation behaviour of the free hydrogen is expected for this sample.

For each cooling rate, four samples with the stated individual hydrogen concentrations were placed in a furnace and heated to a maximum temperature of 347 °C. Subsequent cooling was performed after a hold time of a minimum of 2.5 h. Cooling rates of 150, 12.5, 1.8 and 0.4 °C/h resulting in a test matrix of four cooling rates by four hydrogen concentrations (see table 1). Samples with the highest cooling rate have been subject to free atmospheric cooling, giving a non-linear temperature profile. However, a cooling rate of 150 °C/h was extrapolated from the thermocouple readings. Samples were subsequently cut, polished and etched for preparation for light optical microscopy (LOM) investigations. Micrographs of the full cladding ring were prepared with low

magnification image of the entire cross section to get an overview of the hydride distribution. More detailed micrographs were produced at higher magnification ($\times 10$ and $\times 20$) for different positions of the specimen. An example of a full ring micrograph is shown in figure 1.

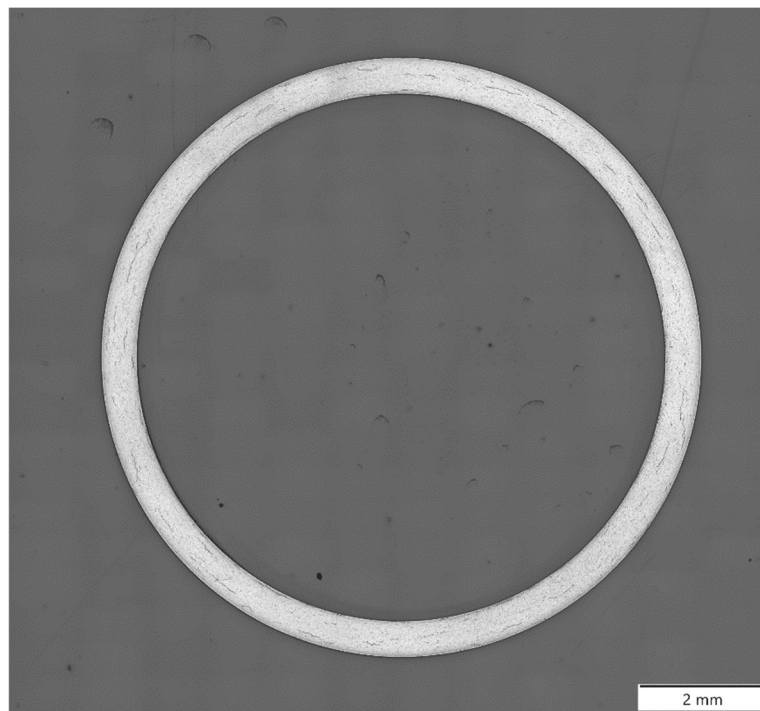


Figure 1 Example of a micrograph of a full ring sample with 96 ppm hydrogen. The micrograph shows no preferred circumferential distribution of hydrides over the full ring sample and throughout the cladding wall thickness.

2.2 Hydrogen Diffusion Experiment

A pre-hydrated cladding tube segment of 190 mm length was used to determine temperature driven diffusion along the axial direction of cladding tubes. The sample was charged with hydrogen using cathodic charging method to reach a concentration of 100 ppm total hydrogen. We observed a gradient in the concentration over the length of the specimen: pre-test hydrogen concentration was measured using HE to be 59 ppm and 98 ppm on the ends.

The segment was placed in a furnace at a maximum temperature of 349 °C on the hot end of the specimen, imposing a constant temperature gradient of 2.59 °C/cm over the whole sample length (48 °C in total) to the cold end of the specimen. The sample has been oriented with its 59 ppm end to the cold side of the furnace.

The static temperature gradient was held for a duration of one month to allow for hydrogen re-distribution according to thermal diffusion along the temperature gradient. Subsequent cool-down results in conservation of the equilibrium hydrogen distribution. The cooling rate can be assumed to be in the range of 150 °C/h but was not measured

because hydride morphology was not in the scope of this experiment. The influence on hydrogen concentration due to morphology changes induced by fast cooling rates (150 °C/h) is negligible. The post-test hydrogen profile was analyzed by cutting the specimen at several positions and determining hydrogen concentrations using HE.

3 Results and Discussion

3.1 Hydride Morphology

Two distinct effects can be derived by systematically analyzing the samples of the hydrogen morphology experiments being the effect of cooling rate on the one hand (micrographs shown in figure 2) and the effect of total hydrogen concentration on the other hand (micrographs shown in figure 3). Both effects are described separately in the following. Samples in the figures were chosen to give best quality pictures. An overview of selected micrograph samples for all cooling rates and hydrogen concentrations is shown in figure 4.

3.1.1 Effect of Cooling Rate

Fast cooling rates promote precipitation of small hydrides nucleus whereas slow cooling rates rather promote hydride growth because sufficient time is available to transport solute hydrogen by diffusion towards the hydride tip for its growth [7, 8, 19–21]. Our experimental results are in line with research in the literature [7, 20, 21]. The evolution of zirconium hydrides with cooling rates can be followed in figure 2 starting on the left side picture at 150 °C/h developing more randomly oriented and distributed short hydrides in huge number. With decreasing cooling rate, number of hydrides decreases to give longer circumferential oriented hydrides. The effect carries on for the lowest cooling rate of 0.4 °C/h developing only few hydrides with considerable length. Generally, the hydrides tend to be circumferentially oriented which is related to the stress free state of the cladding during cooling and the preferred grain orientation of the Zirconium matrix.

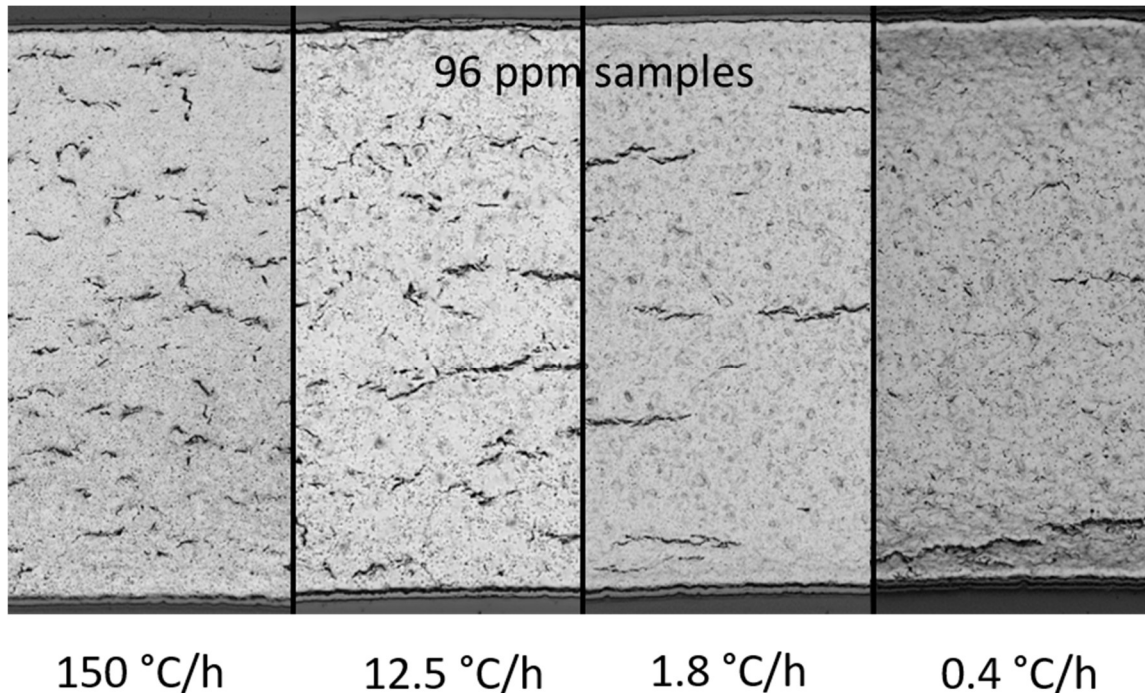


Figure 2: Micrographs of four samples with hydrogen concentration of 96 wt. ppm subject to four different cooling rates. The cladding outside is shown on the top and inside on the bottom of the micrographs. At 150 °C/h hydrides show random orientation with short hydrides, evenly distributed via cladding thickness. At 12.5 °C/h, longer hydrides with random orientation are formed. At 1.8 °C/h, less and longer hydrides are formed in circumferential orientation. At 0.4 °C/h, long hydrides are formed in circumferential direction, leaving hydride depleted zones in the cladding.

Besides number and size of the hydrides formed, figure 4 shows an orientation effect in hydride morphology for the samples with the fastest cooling rate of 150 °C/h. The fast cooling necessitates precipitation, leading to a system governed by kinetic processes [19]. It can be assumed that the preferential orientation of the hydrides in circumferential direction is overcome by the fast cooling rate and the resulting precipitation kinetics. The effect can also be observed to a lesser extent in the second to left column of figure 4 with a cooling rate of 12.5 °C/h.

3.1.2 Effect of total hydrogen concentration

An increased amount of hydrogen leads to an increased amount of zirconium hydrides at a given temperature. However, when it comes to zirconium hydride size, distribution, and orientation, additional aspects play a role. The total hydrogen concentration in zirconium-based alloys is considered in the literature as an important factor for reorientation and the precipitation solvus of hydrogen [9, 10, 22]. At hydrogen contents exceeding the dissolution solvus (TSSd), remaining hydrides influence the precipitation solvus (TSSp) but also the resulting hydride microstructure given at room temperature [10, 11, 22]. Regarding this effect, total hydrogen concentration needs to be considered

in combination with maximum temperature to determine existing hydride structures. Figure 3 shows the four different hydrogen concentrations analyzed in this work at a cooling rate of 1.8 °C/h. It is clearly visible that for the given cooling rate the number of hydrides increases with increasing hydrogen concentration.

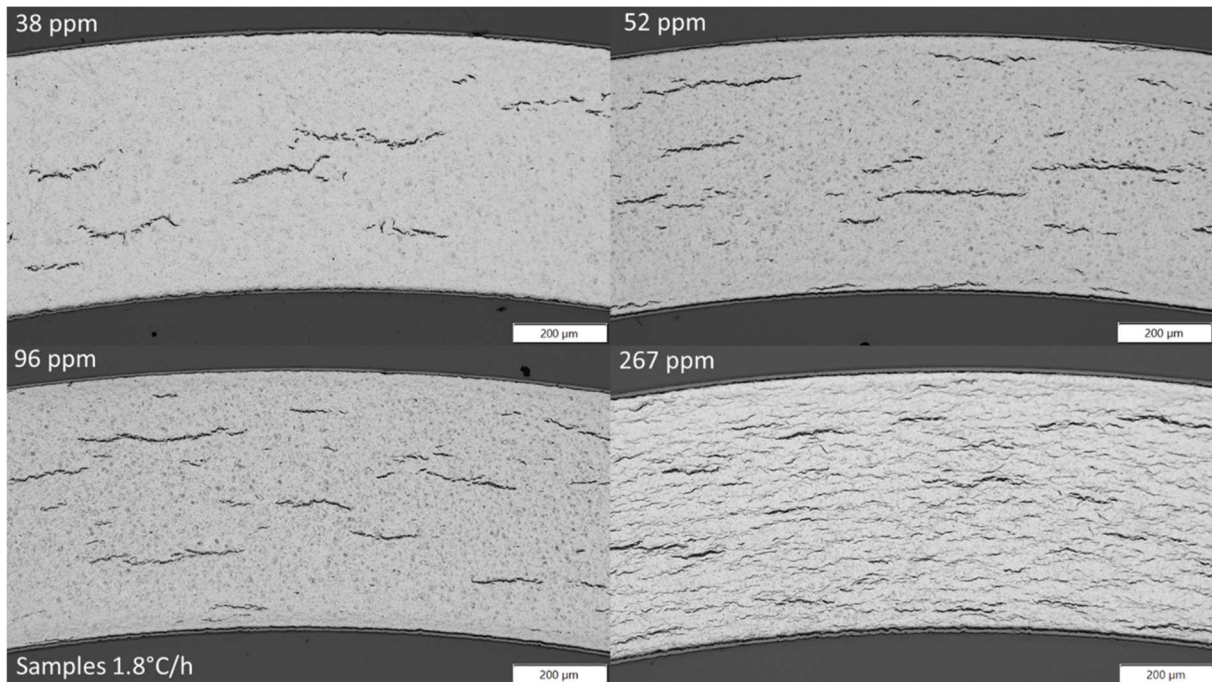


Figure 3 Micrographs of four samples with different hydrogen concentrations subject to a cooling rate of 1.8 °C/h. The 38 wt. ppm sample on the upper left shows few long hydrides, mostly circumferentially orientated. The 52 wt. ppm sample on the upper right shows more hydrides, mostly circumferentially orientated. The 96 wt. ppm sample on the lower left exhibits an increased number of circumferential hydrides. The 267 wt. ppm sample on the lower right shows circumferentially orientated hydrides in two shades. A mesh of fine hydrides appearing in light grey evenly distributed over the cladding and few darker hydrides similar to the other samples are visible.

At hydrogen concentrations corresponding to full dissolution at maximum temperature, increasing hydrogen content results in an increase of hydride density. The effect could be observed for the lower three cooling rates of this work (12.5, 1.8 and 0.4 °C/h, shown in the respective columns of figure 4). However, the fastest cooling rate showed just minor effects of total hydrogen concentration on the number of hydrides formed in the matrix as shown in the left column in figure 4.

Consistently with [19], under full dissolution conditions and at maximum cooling rate of 150 °C/h, figure 4 shows comparable hydride nucleation density independently of hydrogen content.

The highest hydrogen concentrations tested in the sample matrix of 267 ppm depict a sample having considerably higher total hydrogen compared to the TSSd. Using the estimation of [23] to estimate the terminal solid solubility for the dissolution (TSSd)

gives $cTSSD = 116$ ppm at a maximum temperature of 350 °C. Apart from this estimation, it seems to be reasonable to assume the 267 ppm being well above the TSSD concentration [19, and ref. therein]. Therefore, residual hydrides were present at the start of cooling, allowing dissolved hydrogen to attach during sample cooling. The series of specimen with a hydrogen concentration of 267 ppm (lowest row in figure 4) furthermore shows the lowest sensitivity to changes in the cooling rate. This can also be explained by the undissolved zirconium hydrides remaining in the matrix at maximum temperature and pre-determining the number of hydrides to be formed by providing a rather tight distribution of energetically preferred attachment options for dissolved hydrogen during the precipitation process.

All samples of high hydrogen content showed the distribution of some bold zirconium hydrides in between a homogeneous distribution of thinner hydrides. This may be another effect related to existing hydrides at the beginning of sample cooling. However, there is no direct explanation, as new nucleation is unlikely to occur during cooling with existing hydrides and all hydride structures should have been present at maximum temperature, but smaller in size.

It is worth noting, that hydrides in the full ring micrographs are evenly distributed throughout the cladding wall thickness for all combinations of cooling rates and concentrations. A statistical significant distribution of hydrogen accumulation at specific radial positions, e.g. at the inner side of the cladding as shown in Figure 4 for 38 wt. ppm and lowest cooling rate cannot be observed in the full ring images.

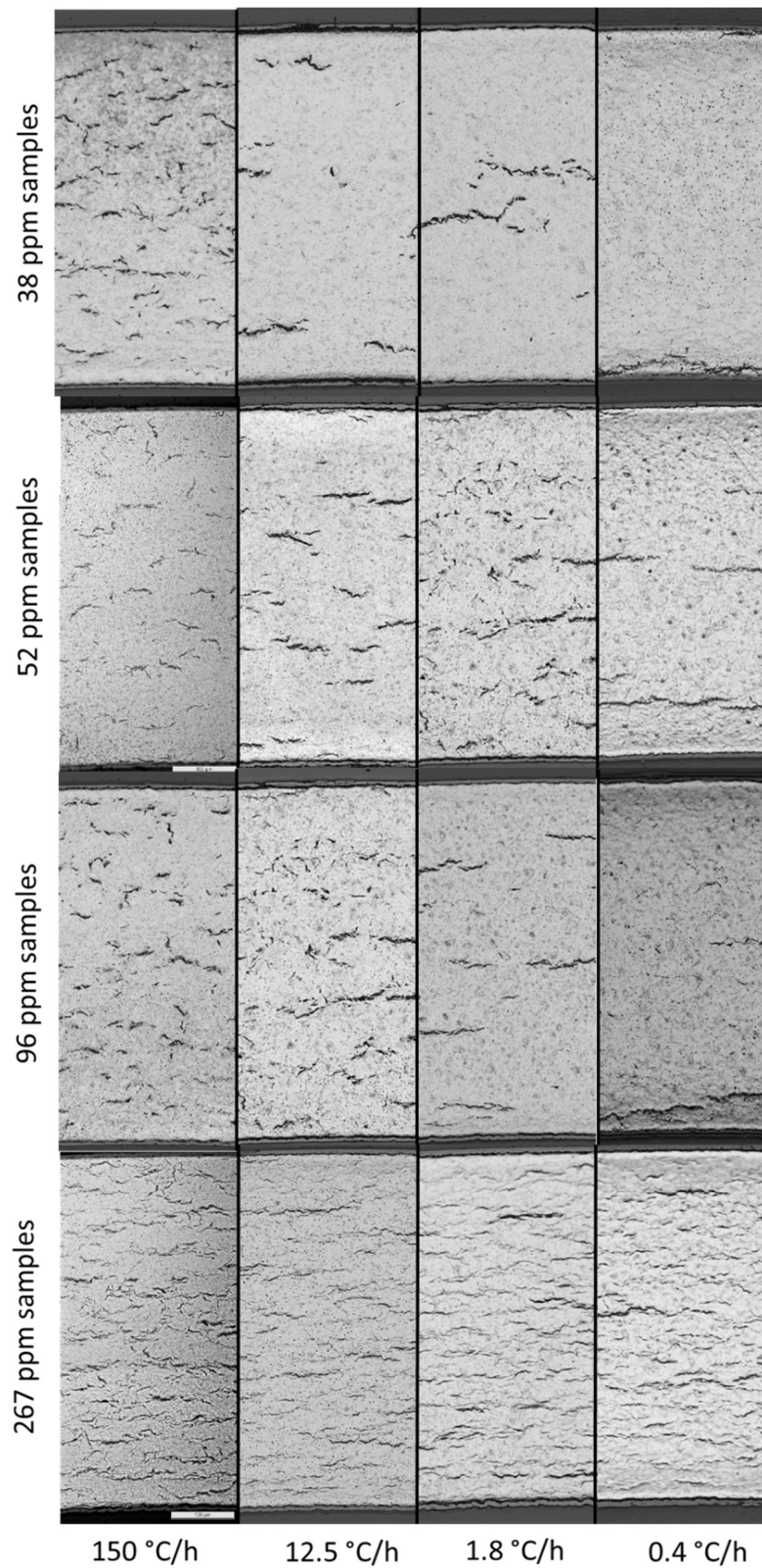


Figure 4 Overview of test matrix for morphology experiments shown as a 4×4 matrix. From left to right column, the cooling rate decreases from 150°C/h to 0.4°C/h. From top to bottom row, the hydrogen concentration increases from 38 wt. ppm to 267 wt.

ppm. Except for the latter one, all samples with 150°C/h show a random orientation, whereas all 267 wt. ppm samples exhibit a fine mesh of circumferential hydrides in light grey with fewer hydrides in darker grey.

3.2 Hydrogen Diffusion

Diffusion of hydrogen in a cladding tube segment of 190 mm length was analysed to determine the temperature driven diffusion in zirconium based cladding. The pre-hydrided sample was heated to a maximum temperature of 349 °C at the hot end of the specimen, imprinting a constant temperature gradient of 2.59 °C/cm to the cold end of the specimen at 301 °C. This assumption of a an axial temperature gradient of the cladding is well in line with actual gradients inside loaded dry casks, cf. [24]. Pre-test hydrogen concentration was measured to be 59 ppm and 98 ppm at the cold (left) and hot (right) end, respectively in figure 5. Post-test hydrogen profile was determined at seven positions of the specimen, see table 2. Results of the hydrogen diffusion experiment are shown in figure 5.

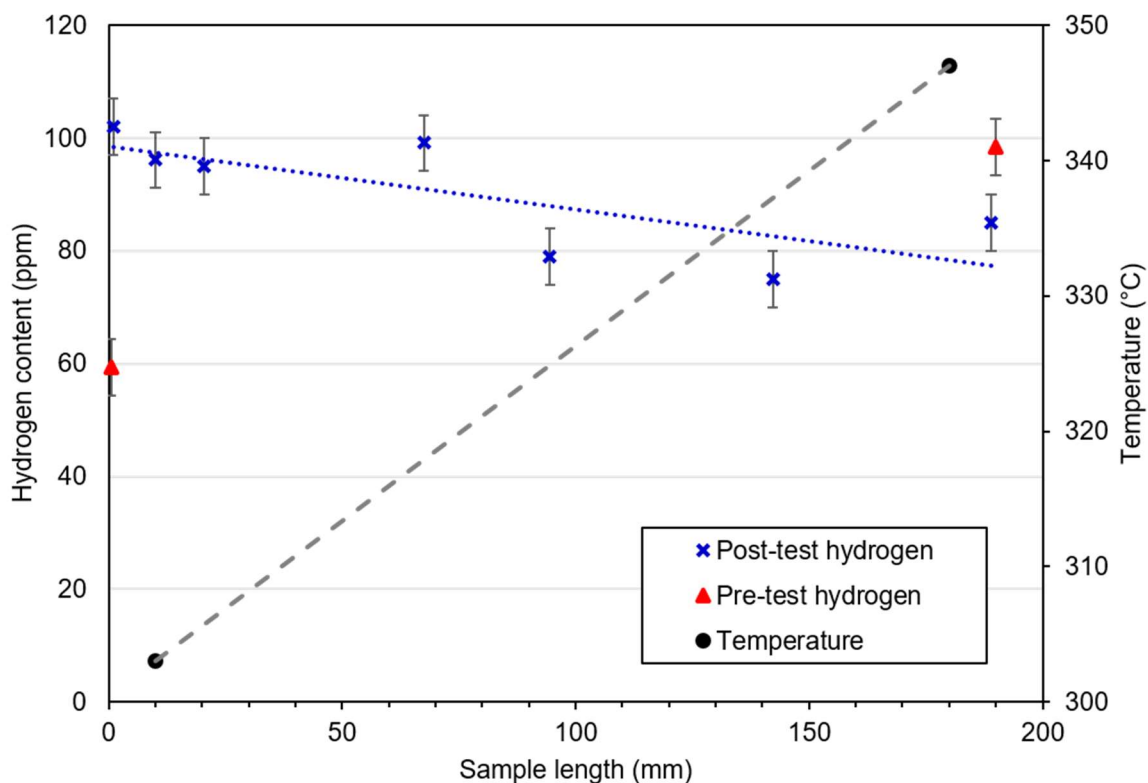


Figure 5 Hydrogen concentration before and after diffusion experiment under constant temperature gradient. The temperature increases from 301 °C on the left side to 349 °C on the right side marked with black dots. The pre-test hydrogen concentration was determined to be 59.33 (±5) wt. ppm on the left end and 98.33 (±5) wt. ppm on the right end of the sample (red triangles). The post-test hydrogen concentration shows an inverted trend, with higher values of 102 (±5)wt. ppm on the left side and 85 (±5) wt. ppm on the right side (blue x-marks).

Position [mm]	Concentration [wt. ppm]	Temperature [°C]
0.5	59 ±5	-
1	102 ±5	301
10	96 ±5	303
20.5	95 ±5	306
67.5	99 ±5	318
94.5	79 ±5	325
142.25	75 ±5	337
189	85 ±5	349
190	98 ±5	-

Table 2 Measured concentrations and temperatures of samples according to cutting position used in diffusion experiments. The pre-test hydrogen determinations at positions 0.5 and 190 mm are marked in light grey. At these positions the temperature has not been measured, since they have not been exposed to the temperature gradient.

Experimental uncertainty is not straight forward to determine. After receiving the samples, three HVE measurements of 1 mm rings each at both ends of the rod have been performed and showed concentrations of 61, 58, 59 ppm and 99, 99, 97 ppm, respectively. Thus we assume a measurement uncertainty of ±5 ppm which is in line with typical uncertainties for the hot extraction method.

The pre-test trend of the hydrogen content, depicting higher concentration (98 ppm) at the hot side and lower concentration at the cold side (59 ppm) is reversed during the test. The temperature gradient of 2.59 °C/cm lead to a redistribution of hydrogen depicting a mean hydrogen concentration difference of 22 ppm over the total sample length. Nevertheless, high measurement uncertainties, as visible in the distinct HE measurements of post-test hydrogen concentration, reduce the overall reliability of the result.

4 Conclusion

This study provides critical insights into the behaviour of hydrogen and unirradiated Zircaloy-4 cladding tubes in which no hoop-stress was applied. By systematically analyzing the effects of cooling rates and hydrogen concentrations on hydride morphology for 16 samples (Fig. 4), as well as examining hydrogen diffusion along the axial direction of cladding tubes (Fig. 5), several key findings have been elucidated.

Firstly, the experiments demonstrate that cooling rates significantly influence hydride morphology. Faster cooling rates result in a higher number of smaller, randomly oriented hydrides, while slower cooling rates produce fewer, larger, and more circumferentially oriented hydrides, as shown in Fig. 4. This kinetic-driven precipitation process highlights the importance of controlling cooling rates to manage hydride formation and distribution within the cladding material.

Secondly, the total hydrogen concentration is a critical factor in determining the number and size of hydrides. Higher hydrogen concentrations lead to an increased number of

of Radioactive Materials

hydrides, although the impact of hydrogen concentration diminishes at the fastest cooling rates. The presence of residual hydrides at higher concentrations also affects the subsequent precipitation behaviour, resulting in a more uniform distribution of hydrides with some prominent larger hydrides.

The hydrogen diffusion experiments reveal that temperature gradients significantly drive hydrogen redistribution along the cladding tube (see Fig. 5). The observed reversal of the hydrogen concentration gradient during the test underscores the effectiveness of thermal diffusion in altering hydrogen profiles. However, the inherent uncertainties in hydrogen measurement highlight the need for precise and repeated analyses to ensure the reliability of the results.

In summary, this research is in line with [7, 8, 12–14, 19–21] and enhances our understanding of hydrogen behaviour in nuclear fuel cladding, providing valuable data to improve predictions for hydrogen diffusion and precipitation. The findings not only address considerations for unirradiated cladding tubes but also lay the groundwork for the necessary future studies on irradiated fuel rods. To describe the hydrogen behaviour during the dry storage of irradiated fuel assemblies, the hydride morphology has to be investigated for irradiated fuel rods with prototypical radiation histories including hoop stresses.

However, experimental investigations on irradiated fuel rods are more complex to conduct due to the high radioactivity. Also, samples of irradiated fuel rods in the laboratories are more precious and experiments should be planned to a greater detail. Based on the work at hand and knowing that the actual cooling rates in dry storage are much lower than the ones investigated in this work, we recommend to use at least cooling rates below 0.4 °C/h to investigate realistic hydride morphologies.

5 Acknowledgements

The authors would like to thank all involved colleagues at Studsvik Nuclear AB for valuable discussions. We also thank Marc Péridis and Robert Brüninghoff who were involved in this work during an earlier stage.

6 Literature

- [1] A.T. Motta, A. Couet, R.J. Comstock, Corrosion of zirconium alloys used for nuclear fuel cladding. *Annual Review of Materials Research* **45** (Volume 45, 2015), 311–343 (2015). <https://doi.org/https://doi.org/10.1146/annurev-matsci-070214-020951>. URL <https://www.annualreviews.org/content/journals/10.1146/annurev-matsci-070214-020951>
- [2] M.P. Puls, *The Effect of Hydrogen and Hydrides on the Integrity of Zirconium Alloy Components* (Springer, London, 2012). <https://doi.org/https://doi.org/10.1007/978-1-4471-4195-2>
- [3] A.T. Motta, L. Capolungo, L.Q. Chen, M.N. Cinbiz, M.R. Daymond, D.A. Koss, E. Lacroix, G. Pastore, P.C.A. Simon, M.R. Tonks, B.D. Wirth, M.A. Zikry, Hydrogen in zirconium alloys: A review. *Journal of Nuclear Materials* **518**, 440–460 (2019). <https://doi.org/https://doi.org/10.1016/j.jnucmat.2019.02.042>. URL <https://www.sciencedirect.com/science/article/pii/S0022311518316763>

- [4] A.A. Plyasov, V.V. Novikov, Y.N. Devyatko, A review of hydride reorientation in zirconium alloys for water-cooled reactors. *Physics of Atomic Nuclei* **83**, 1407 – 1424 (2020). URL <https://api.semanticscholar.org/CorpusID:234554884>
- [5] K. Kese. Hydride re-orientation in zircaloy and its effect on the tensile properties (2004). URL <https://api.semanticscholar.org/CorpusID:244919227>
- [6] E. Lacroix, A. Motta, J. Almer, Experimental determination of zirconium hydride precipitation and dissolution in zirconium alloy. *Journal of Nuclear Materials* **509**, 162–167 (2018). <https://doi.org/https://doi.org/10.1016/j.jnucmat.2018.06.038>. URL <https://www.sciencedirect.com/science/article/pii/S0022311517317798>
- [7] Q. Auzoux, P. Bouffieux, A. Machiels, S. Yagnik, B. Bourdilliau, C. Mallet, N. Mozzani, K. Colas, Hydride reorientation and its impact on ambient temperature mechanical properties of high burn-up irradiated and unirradiated recrystallized zircaloy-2 nuclear fuel cladding with an inner liner. *Journal of Nuclear Materials* **494**, 114–126 (2017). <https://doi.org/https://doi.org/10.1016/j.jnucmat.2017.07.022>. URL <https://www.sciencedirect.com/science/article/pii/S002231151730209X>
- [8] J.M. Lee, H.A. Kim, D.H. Kook, Y.S. Kim, A review of factors influencing the hydride reorientation phenomena in zirconium alloy cladding during long-term dry storage. *Korean Journal of Metals and Materials* **56**(2) (2018). <https://doi.org/10.3365/KJMM.2018.56.2.79>
- [9] O. Zanellato, M. Preuss, J.Y. Buffiere, F. Ribeiro, A. Steuwer, J. Desquines, J. Andrieux, B. Krebs, Synchrotron diffraction study of dissolution and precipitation kinetics of hydrides in zircaloy-4. *Journal of Nuclear Materials* **420**(1), 537–547 (2012). <https://doi.org/https://doi.org/10.1016/j.jnucmat.2011.11.009>. URL <https://www.sciencedirect.com/science/article/pii/S0022311511009615>
- [10] Z. Pan, I. Ritchie, M. Puls, The terminal solid solubility of hydrogen and deuterium in zr-2.5nb alloys. *Journal of Nuclear Materials* **228**(2), 227–237 (1996). [https://doi.org/https://doi.org/10.1016/S0022-3115\(95\)00217-0](https://doi.org/https://doi.org/10.1016/S0022-3115(95)00217-0). URL <https://www.sciencedirect.com/science/article/pii/S0022311595002170>
- [11] J.S. Kim, T.H. Kim, K. min Kim, Y.S. Kim, Terminal solid solubility of hydrogen of optimized-zirlo and its effects on hydride reorientation mechanisms under dry storage conditions. *Nuclear Engineering and Technology* **52**(8), 1742–1748 (2020). <https://doi.org/https://doi.org/10.1016/j.net.2020.01.022>. URL <https://www.sciencedirect.com/science/article/pii/S1738573319307004>
- [12] S.D. Kim, Y. Rhyim, J.S. Kim, J. Yoon, Characterization of zirconium hydrides in zircaloy-4 cladding with respect to cooling rate. *Journal of Nuclear Materials* **465**, 731–736 (2015). <https://doi.org/https://doi.org/10.1016/j.jnucmat.2015.07.006>. URL <https://www.sciencedirect.com/science/article/pii/S0022311515300921>
- [13] S.J. Min, M.S. Kim, K.T. Kim, Cooling rate- and hydrogen content-dependent

hydride reorientation and mechanical property degradation of zirconium alloy claddings. *Journal of Nuclear Materials* **441**(1), 306–314 (2013). <https://doi.org/10.1016/j.jnucmat.2013.06.006>. URL <https://www.sciencedirect.com/science/article/pii/S0022311513008271>

[14] R. Birch, S. Wang, V.S. Tong, T.B. Britton, The effect of cooling rate and grain size on hydride microstructure in zircaloy-4. *Journal of Nuclear Materials* **513**, 221–225 (2019). <https://doi.org/10.1016/j.jnucmat.2018.11.011>. URL <https://www.sciencedirect.com/science/article/pii/S0022311518314065>

[15] J. Kearns, C. Woods, Effect of texture, grain size, and cold work on the precipitation of oriented hydrides in zircaloy tubing and plate. *Journal of Nuclear Materials* **20**(3), 241–261 (1966). [https://doi.org/10.1016/0022-3115\(66\)90036-5](https://doi.org/10.1016/0022-3115(66)90036-5). URL <https://www.sciencedirect.com/science/article/pii/0022311566900365>

[16] ASTM International. Standard specification for wrought zirconium alloy seamless tubes for nuclear reactor fuel cladding (2022). URL <https://www.astm.org/b0811-13r22e01.html>. ASTM B811-13(2022)e1

[17] Eltra GmbH. Elementrac OH-p2 - Product data sheet (2024). URL <https://www.eltra.com/products/onh-analyzers/oh-p/>. 18th July 2024

[18] Leica Microsystems Wetzlar GmbH. Leica MEF4 A / MEF4 M - Product data sheet. URL <https://www.leica-microsystems.com>. 18th July 2024

[19] P. Kaufholz, M. Stuke, F. Boldt, M. Péridis, Influence of kinetic effects on terminal solid solubility of hydrogen in zirconium alloys. *Journal of Nuclear Materials* **510**, 277–281 (2018). <https://doi.org/10.1016/j.jnucmat.2018.08.011>. URL <https://www.sciencedirect.com/science/article/pii/S0022311518305968>

[20] A.M. Alvarez, R.K. Andersson, J. Stjärnsäter, J. Karlsson, P. Tejlund, F.M. Boldt, P. Kaufholz, On the effect of internal pressure and cooling rate on the hydride reorientation in optimized zircaloy cladding. *Proceedings of TopFuel 2024* (2024). Paper A0168 presented at the TopFuel Conference 2024 29th Sept–3rd Oct 2024

[21] A.M. Alvarez, J. Stjärnsäter, J. Karlsson, B. A., P. Tejlund, K.D. Johnson, R. Josek, Evaluation of the hydride reorientation behavior for zircaloy-2 liner cladding with high hydrogen content during interim dry storage conditions. *Zirconium in the nuclear industry: 20th international Symposium* pp. 673–694 (2023). <https://doi.org/10.1520/STP164520220013>. *Zirconium in the Nuclear Industry: 20th International Symposium*, ASTM International, 2023

[22] K. Une, S. Ishimoto, Dissolution and precipitation behavior of hydrides in zircaloy-2 and high Fe zircaloy. *Journal of Nuclear Materials* **322**(1), 66–72 (2003). [https://doi.org/10.1016/S0022-3115\(03\)00320-9](https://doi.org/10.1016/S0022-3115(03)00320-9). URL <https://www.sciencedirect.com/science/article/pii/S0022311503003209>

[23] J.G. Bang, J.H. Baek, Y.H. Jeong. Determination of terminal solid solubility of hydrogen in zirconium alloys (2004). Paper presented at the 2004 Korean Nuclear Society Autumn Meeting p.1028-1029

[24] H. Akkurt, D. Richmond, M. Stuke, *International Thermal Modeling Benchmark Project – Phase I Results; An Extended Storage Collaboration Program Activity*. Technical Report 3002023976 (EPRI, California, USA, 2022). <https://doi.org/>
<https://www.epri.com/research/products/000000003002023976>